Application of the Force Balance Model and Fractal Scaling Analysis for Size Estimation of the Complex-Agglomerates in a Conical Fluidized Bed

Bahramian, Ali Reza*[+]

Chemical Engineering Department, Hamedan University of Technology, P. O. Box 65155 Hamedan, I.R. IRAN

ABSTRACT: *The size estimating of fluidized Titania agglomerates in a conical fluidized bed was studied by force balance model and fractal scaling analysis. The primary size of titania Nano Particles (NPs) was 21 nm, while for complex agglomerates was in the size range of several hundred micrometers. The formation mechanism of simple-agglomerate and complex-agglomerate structures was studied experimentally. The size distribution and morphology of agglomerates were determined by advanced laser dynamic imaging and scanning electron microscopy. The AFM-nanoindentation test was used to determine the elastic modulus of agglomerates with porous structures. The size distribution of Titania NP agglomerates was estimated by the fractal analysis through the relationship between the number of particles and gyration diameter. The fractal exponent obtained from the power-law scaling of agglomerates and the complex agglomerate sizes were determined experimentally and theoretically. A simple theoretical model was applied to estimate the complex agglomerates' size based on the equilibrium of the separation and cohesion forces. The proposed model showed satisfactory results compared with the experimental data. The results of the present study can help to determine the critical gas velocity in achieving the desired agglomerate size of Titania NPs.*

KEYWORDS: *Fluidization, Size estimation, Nanoparticle agglomerates, Force balance model, Fractal scaling analysis.*

INTRODUCTION

Fluidization of nanoparticles (NPs) is associated with complexity due to the presence of interparticle forces including the capillary forces and van der Waals and electrostatic forces [1-3]. Conical fluidized beds are known as alternative tools for fluidization of heavy and sticky ultrafine particles in the chemical, dyes, and pharmaceutical industries due to high contact efficiency between the gas and particles [4]. The performance of conical fluidized beds is related to the size, density, porosity, and morphology of primary NPs and their formed agglomerates, and also the bed hydrodynamic characteristics. The minimum fluidization velocity U_{mf}, depends on the material properties such as the size, density, and shape of the particles and the fluidizing gas

* *To whom correspondence should be addressed.*
+ E-mail: bahramian@hut.ac.ir
1021-9986/2021/3/955-970 *16/$/6.06*

properties. However, the other parameters such as the bed geometry, aspect ratio, and distributor design can be effective in the fluidization characteristics [5]. As the material density is increased, the U_{mf} is increased as well [2, 4]. *Nam et al.* [1] showed that the U_{mf} of the bed containing NP agglomerates was several orders of magnitude higher than the primary NPs. *Sun* and *Grace* [6] studied the effect of the Particle Size Distribution (PSD) on the performance of a fluidized bed reactor with different hydrodynamic regimes including bubbling, slugging, turbulent and fast fluidization regimes. Their results showed the transition regime from bubbling (or slugging) to turbulent fluidization for bed with the wide PSD were happened earlier than the narrow PSD. Depending on Geldart's classification and superficial gas velocity, particles tend to fluidize in homogeneous, bubbling, slugging or spouting beds [7].

The physical properties of agglomerates can change during fluidization because of the agglomerates continuously break and aggregate in a bed, especially when a high amount of NPs loaded in the bed [8,9]. The primary NPs tend to stick together and form aggregates with a few hundred nanometers [10]. The aggregates coalesce into larger structures by physical interparticle forces to form simple-agglomerates with porous structure and a few microns in size [11, 12]. The simple-agglomerates stick into large structures called complex agglomerates with hundreds of microns in size. The morphology of complex-agglomerates is affected by the fluidizing gas or collisions of particles with each other [13]. *Yao et al.* [2] studied the SiO_2 NPs in a fluidized bed in three categories of the aggregates (1-100 nm), simple-agglomerates (1-100 μm), and complex-agglomerates (200-400 μm). *Hakim et al.* [14] was investigated the fluidization behavior of NPs based on the ratio of intra-aggregate force to inter-aggregate cohesive forces in a fluidized bed. The aggregation of cohesive NPs firstly occurred inside the fluidized bed through dynamic and stationary forces. Dynamic aggregation occurs due to a dynamical equilibrium between the cohesive and inertial forces, where aggregates are formed and broken continuously because of the collision forcein the bed. Stationary aggregation of NPs takes place because of the cohesive forces, including loading conditions during handling and storage. *Hakim et al.* [14] showed that the ratio of the intraparticle forces, which hold NPs together, to interparticle forces, which are the cohesive forces between the simple-agglomerates, is a key factor in the determination of the agglomerates size. A fragile and porous structure of simple-agglomerates can challenge the validity of structural morphological results and the repeatability of its results. An elasticity measurement could help to study the mechanical and structural properties of agglomerates. Atomic Force Microscopy (AFM) is a well-known method to investigate the elasticity and Young's modulus of soft matter based on the nanoindentation analysis through the interaction between the AFM tip and sample [15, 16].

The structure of agglomerates in each step could be characterized by their fractal dimension [17, 18]. The fractal analysis illustrates the size distribution of NPs when they form agglomerate structures and the mechanism of agglomeration. A decreasing the fractal dimension can be led to an increase in the porous structure of the agglomerates. *Fabre et al.* [19] found that the aggregates have a fractal dimension (D_f) of ~1.5, while the simple-agglomerates with highly porous clusters have a fractal dimension between 2.6 and 3, corresponding to the reaction-limited mechanism. They also found that the complex-agglomerates exhibit a fractal dimension between the 1.8 and 2.2, corresponding to the diffusion-limited mechanism [20]. *Nam et al.* [1] studied the hydrophobic silica NP agglomerates with the size of 20-40 μm in an expanded fluidized bed. The results obtained from different bed heights showed that complex-agglomerates could be broken into simple-agglomerates during fluidization. They reported D_f=2.5, which was corresponded to the diffusion-limited agglomeration (DLA) mechanism for complex-agglomerates. The mentioned mechanism creates cluster-cluster structures with D_f=1.80, while D_f= 2.50 represents the particle-cluster structure of the DLA mechanism. A D_f=3.0 was reported for clusters created by a particle-cluster ballistic aggregation and reaction-limited mechanism [1, 17, 18]. Valverde and Castellanos [21] showed the fluidized silica, zirconia, and iron oxide NP agglomerates have a D_f=2.57. They found that the fractal dimension correlated well with the fluidization characteristics of the bed including type and velocity of inlet gas, and initial static bed height H_0, where increasing D_f was related to decreasing fluidization characteristics.

The structure of agglomerate is generally defined by the fractal dimension [17, 18]. The number of particles N_p in the fractal structures formed by mono-disperse particles of the size, d_p, is determined by the well-known scaling law [22]:

$$N_p = k_n \left(\frac{d_{agg}}{d_p} \right)^{D_f} \quad (1)$$

The agglomerate density ρ_{agg}, by regarding the power of ratio d_{agg}/d_p, is given by [2, 9]:

$$\rho_{agg} = \rho_p k_n \left(\frac{d_{agg}}{d_p} \right)^{D_f - 3} \quad (2)$$

where d_{agg} is the agglomerate diameter, ρ_p is the density of particles and k_n is a prefactor value. The term of prefactor was applied to offer a physical concept to the expression of the limits of the individual NP and particularly large cluster structures. Typically, $D_f \approx 1$ is found for sticky particles, while $D_f \approx 3$ is reported for compact agglomerates and $1<D_f<2$ for porous structures [19]. *Quintanilla et al.* [23] used an image analysis procedure to estimate the fractal dimension of fluidized NP agglomerates larger than ~100 μm. They showed that the bed expansion is determined by the mean values of the size and density of agglomerates. They also used an average density and $k_n=1$ to characterize the bed expansion ratio and the fractal dimension of agglomerates. The result of power-law scaling showed a $D_f=2.5$ for the agglomerates in the range size of ~100-300 μm [23]. *Sorenson et al.* [24] found that the prefactor of the fractal structures by the assumption of $k_n=1$ has a correct $N_p=3$, which corresponds to the linear configuration of three monomers. *Jiang* and *Logan* [25] showed the k_n is related to the packing factor and the ratio of the shape factor and primary NPs. *Ehrl et al.* [22] studied the geometry of micron-sized agglomerates obtained from rigid monodisperse primary particles in the $2.2<D_f<3$ range. They obtained a power-law model for the calculation of the prefactor value according to $k_n=4.46\ D_f^{-2.08}$, which resulted in $k_n \sim 1$ for $D_f=2.0$ [22]. These results showed the assumption of $k_n=1$ provides a reasonable result for the mono-dimensional clusters.

The main challenge in estimating the fluidized agglomerates size was related to the simple-agglomerate size, d^*, resulted from fragmentation and recombination of simple-agglomerates. When the size of agglomerates increases, the acting shear force on an individual NP stuck to the outer layer of the agglomerate is given by [17, 21, 23, 25]:

$$F_s \approx W_p\, k_{agg}^{D^*+2} \quad (3)$$

where W_p is the particle weight and D^* is the global fractal dimension of the simple-agglomerates. Zhou and Li [27] determined the maximum displacement of NP agglomerates and derived a theoretical equation to predict the collision force of two identical spherical agglomerates during fluidization. This property defines the size distribution and elasticity of porous fragile agglomerates formed into the fluidized bed is affected based on the type of collisions of particles and the fluidization parameters. Achievement of the agglomerate size in fluidized bed due to its high importance has been less studied in previous literature. The use of the conical fluid bed, due to its unique properties, can be considered as a good solution for achieving the minimum agglomerate size of NPs.

The objective of the present study is the size estimating of fluidized Titania NP agglomerates in a conical fluidized bed based on the force balance model and the fractal scaling analysis. The formation mechanism of agglomerates was studied experimentally. The size, distribution, and morphology of agglomerates were determined by laser imaging and scanning electron microscopy (SEM) analysis. Young's moduli of the agglomerates were studied by the AFM-based nanoindentation technique. The equilibrium size and size distribution, and agglomeration mechanism of Titania NPs were estimated by the fractal dimension analysis. A theoretical model was proposed based on the equilibrium of separation and cohesion forces. The power-law scaling of agglomerates was used to calculate the fractal exponent and consequently determine the size of complex-agglomerates. The proposed model showed good predicts in size estimating of complex-agglomerates in comparison with the experimental data.

EXPERIMENTAL SECTION

Materials

Dry Titania hydrophilic NPs with a mean size of 21 nm belonging to the C group of Geldart's classification were applied in the experiments. The density of NPs was 3900 kg/m^3, while their bulk density was about 5%

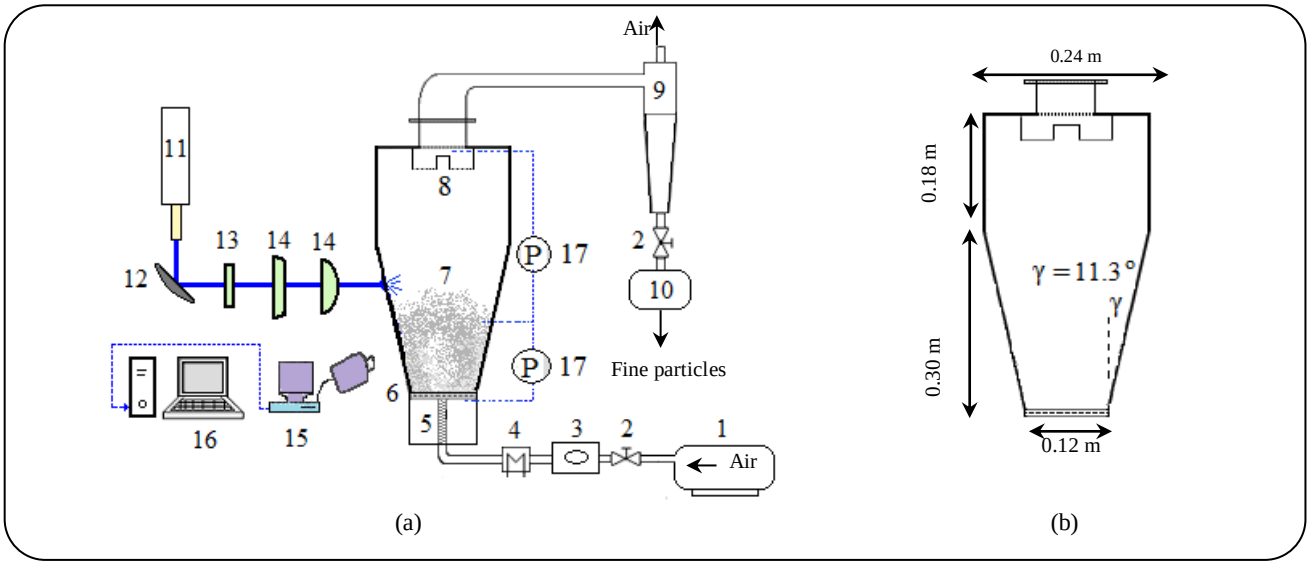

Fig. 1: Compressor, 2 Needle valves, 3 Flow meter, 4 Heat element, 5 Moisture adsorbent, 6 Gas distributor plate, 7 Bed particles, 8 Bag filters, 9 Cyclone, 10 Receiver, 11 Laser light source, 12 Mirror, 13 Filter, 14 Cylindrical and focusing lenses, 15 CCD camera, 16 Computer and data processing, 17 Differential pressure transducers.

of the particle density. An initial static bed height, H_0, of 0.04 m was used for all experiments. The experiments were repeated three times to ensure the reproducibility of the outcomes.

Apparatus and Equipment

The fluidization experiments were performed in a conical fluidized bed unit with a transparent vessel (STREA-1, Niro Aeromatic Co.). A stainless steel gas distributor plate (pore size of 10 µm and thickness of 3 mm) was used to prevent particle leakage from the bed. A bag filter (pore size of 0.45 µm), was applied to the filtering of the ultrafine particles in the exit. Pulsed blow-back of gas led to retain the ultrafine particles to the bed during fluidization. Figs. 1a and 1b are shown the schematic view of the experimental setup and dimensions of the conical bed.

Fluidization Experiments and Imaging

The fluidization experiments were investigated in a conical vessel by nitrogen gas and airflow at ambient temperature. All experiments were carried out once, as the gas velocity (U_g) increased from static state to the fully fluidized bed (U_g=1.0 m/s), and then from the fully fluidized state to the initial state. The gas flow rate was controlled by a needle valve and measured by a rotameter. The pressure fluctuations of the bed were determined by a piezoelectric pressure transducer (type 7261, Kistler). The probe of the pressure transducer is flush-mounted to the inner wall of the conical bed just 0.1 m above the distributor plate in accordance in the literature [28].

The transient bed collapse was captured after shutting off the gas flow by a digital high-speed CCD camera (Ophir-Spiricon Inc. Model: BA 150, pixel resolution: 640 × 480, pixel size: 16 µm, 30 images/s). A Q-switched solid-state laser (photon energy: 200 mJ/pulse) was used as a light source and coupled with a CCD camera. The beam of the laser under the wavelength of 1064 nm and a frequency rate of 10 Hz enters the bed. All images were obtained from the zone near to the upper bed surface as called "splash zone". A lens with variable power magnification between 2.5 and 10 illustrated a region (25×25 mm^2). An image processing method by ImageJ software (version 1.49) was used to analyze the results. The size and morphology of the Titania NPs and their agglomerates were examined by SEM (Cam Scan MV2300). To prepare the samples, the sieve test was used to separate the agglomerates with different sizes. Fig. 2 shows the typical laser image of Titania NP agglomerated at the splash zone of the fluidized bed by nitrogen at U_g=1.0 m/s. Two series of the results, including 25 frames divided by 50 ms intervals, were recorded. The time interval between the two datasets was select to 10 min, based on a required approximate time (~7-10 min) that the

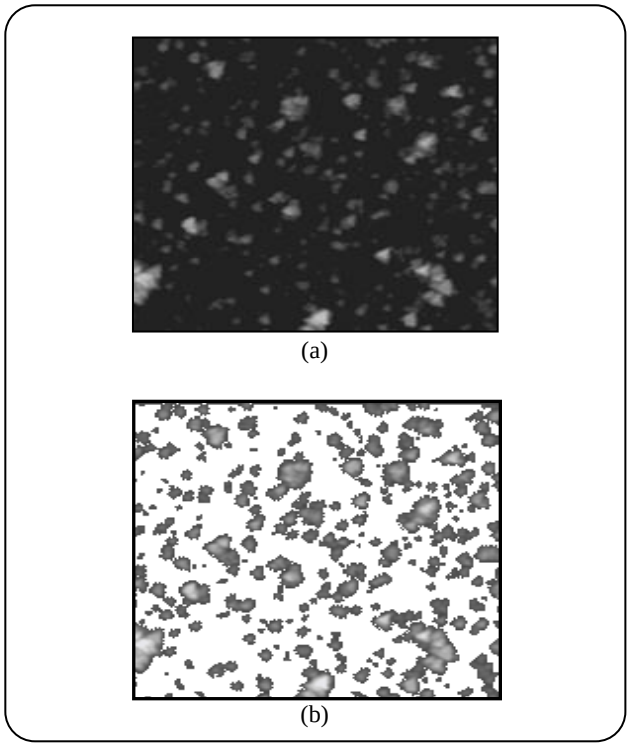

Fig. 2: The image processing of the bed fluidized by airflow at U_g=1.0 m/s. (a) Original image, (b) Threshold image with selected agglomerates.

bed reaches again its U_{mf}. This finding was achieved through 5 repeated tests. The original image and threshold image with selected agglomerates were shown in Figs. 2a and 2b, respectively. The dynamic breakage and reunion process of the agglomerates was determined dynamically through advanced laser dynamic imaging and ImageJ analysis software.

Young's moduli of the agglomerates were studied by the AFM-based nanoindentation technique. Nanoindentation analyses were done by the dynamic contact module of an AFM apparatus (DME Dual Scope). The nanoindentation tests were carried out by a Berkovich diamond indenter (maximum applied loading of 50 mN). The stiffness measurement as a function of indentation depth was applied in the experiments. The tip indenter was regularly loaded and unloaded under a constant frequency of 80 Hz. Young's modulus was determined based on the loading curve, called the load-displacement curve [14, 27]. The force constant and scanning velocity in the normal direction were fixed at 42 N/m and 0.2 μm/s, respectively. To perform force spectroscopy analysis, particles dissolved in the methanol and then obtained solution coated on the film. The distinct points of the films were selected to obtain the force-displacement curve. More information about fluidization procedure and force spectroscopy analysis is available in the literature [29-31].

THEORETICAL SECTION

The fractal dimension of agglomerates with different sizes and physical properties was determined to find the difference between subclasses. To determine the fractal dimension, the number of NPs in each of agglomerates (simple-agglomerates and complex-agglomerates) was represented as a function of gyration diameter d_{gyr} and maximum projected diameter d_c [32]:

$$\frac{d_c}{d_{gyr}} = 1.5 \pm 0.05 \tag{4}$$

A detailed correlation for Stoke's regime gives a similar result [31]:

$$\frac{d_c}{d_{gyr}} = \left(\frac{D_f + 2}{D_f}\right)^{1/2} \tag{5}$$

Size Estimating Model

A force balance modeling was implied to estimate the agglomerate size of Titania NPs [33]. The dynamic equilibrium in the size of two agglomerates was achieved by the equilibrium between the sum of the separation and cohesive forces. The collision forces (F_{col}); drag force (F_D), and gravitational force (F_g) known as separation forces, while van der Waals force (F_{vdW}), the electrostatic force (F_{elec}) and capillary force (F_C) identified as the cohesive forces. Fig. 3 illustrates the schematic picture of the separation and the cohesive forces acting on fluidized NP agglomerates. The size of NP agglomerates was attained by a force balance model, in which the sum of the separation forces is in equilibrium with the cohesive forces:

$$F_{col} + F_D + F_g = F_{vdW} + F_{elec} + F_C \tag{6}$$

In a dry powder, only F_{vdW} and F_{col} are acting as main forces to simplify the complexity of fluidized Titania NP agglomerates. A simple force balance equation was described by [33]:

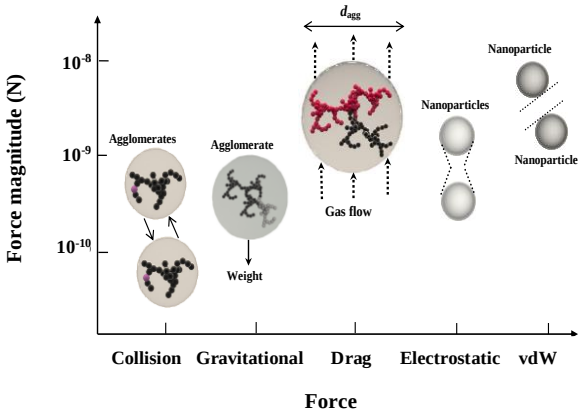

Fig. 3: The schematic diagram of the separation and cohesive forces acting on fluidized agglomerate.

$$F_{col} = F_{vdW} \tag{7}$$

The elasticity theory was used for determining the agglomerates collision force. Owing to the dynamic behavior of the fluidized bed, agglomerate structures were continuously adhering to each other and breaking. It could be assumed that the formed agglomerates were identical spheres colliding in the bed [34]:

$$F_{col} = 0.166\left(\frac{\pi u_{col}^{6}\rho_{agg}^{3}}{k^{2}}\right)^{1/5} d_{agg}^{2} \tag{8}$$

where ρ_{agg} is the agglomerate density, d_{agg} is agglomerate size, u_{col} is relative collision velocity of the agglomerates and k is represented by:

$$k = \frac{1-\nu^{2}}{\pi H_{r}} \tag{9}$$

H_r is Young's modulus of agglomerate calculated by [32]:

$$H_{r} = 17.1\varphi^{4}\left(\frac{E_{p}\Gamma}{d_{agg}}\right)^{1/3} \tag{10}$$

where Γ represents the work of adhesion, and d_p is the diameter of NPs. The attraction force between two atoms and molecules includes the interaction between them representing the van der Waal's force. By assumption of non-elastic interaction, F_{vdW} could be expressed as [35]:

$$F_{vdW} = \frac{h_{w}^{2}\varphi^{2}d_{agg}}{16\pi\delta^{2}}\left(1+\frac{h_{w}\varphi}{8\pi^{2}\delta^{3}H_{r}}\right) \tag{11}$$

Where h_w is the Lifshitz-van der Waals constant ($h_w = 4/3\pi.A_H$), φ is the volume fraction of the agglomerate, d_{agg} is the agglomerate diameter, and δ is the contact distance that typically selected as 0.4 nm [35]. The value of Hamaker constant (A_H) was reported to 15.3×10^{-20} J for Titania NPs in the air at 298 K [36]. Assuming that the first parenthesis of Eq. 11 could be ignored, the force difference in the model becomes:

$$\Delta F = \left(\frac{h_{w}^{3}\varphi^{3}}{128\pi^{3}\delta^{5}H_{r}}\right)d_{agg} - 0.166\left(\frac{\pi u_{col}^{6}\rho_{agg}^{3}}{k^{2}}\right)^{1/5} d_{agg}^{2} \tag{12}$$

The force balance could be simplified to the following form:

$$\Delta F = A\,d_{agg} - B\,d_{agg}^{n} \tag{13}$$

where A is corresponding to the constant term, while the values of B and n were related to the fluidized bed characteristics. To estimate the size distribution, a model was obtained through the determination of agglomerate size, d_{agg}, at zero and maximum force difference (ΔF). Based on this procedure, the d_{agg} at the mode ($d_{agg\,(Mode)}$) and variation point ($d_{agg\,(Max)}$) were obtained theoretically. For the agglomerate bubbling fluidization (ABF) and agglomerate particulate fluidization (APF) flow regimes the constant value of n is corresponding to 2 and 22/5, respectively [27, 33]. The force balance for ABF regime could be introduced in the following form:

$$\Delta F = 0 = A\,d_{agg} - B\,d_{agg}^{2} \longrightarrow d_{agg(Mode)} = (A/B) \tag{14}$$

$$\frac{d\Delta F}{d\,d_{agg}} = 0 = A - 2B\,d_{agg} \longrightarrow d_{agg(Max)} = (A/2B) \tag{15}$$

The results for the APF regime have expressed in the following equations:

$$\Delta F = 0 = A\,d_{agg} - B\,d_{agg}^{22/5} \longrightarrow d_{agg(Mode)} = (A/B)^{5/17} \tag{16}$$

$$\frac{d\Delta F}{d\,d_{agg}} = 0 = A - (22/5)B\,d_{agg}^{17/5} \longrightarrow \tag{17}$$

$$d_{agg(Max)} = (A/B)^{5/17}(5/22)^{5/17}$$

The ratio of A/B includes the Hamaker constant, Young's modulus, volume fraction and relative collision velocity of the agglomerates.

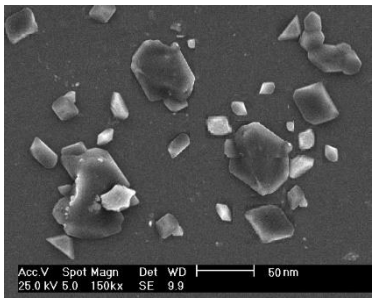

(a)

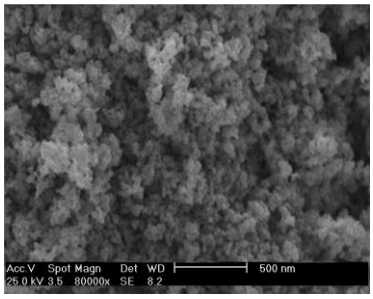

(b)

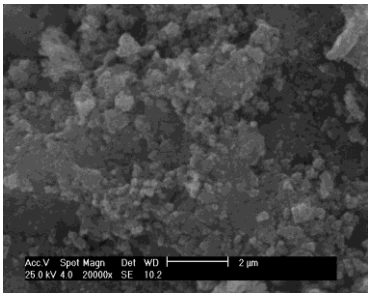

(c)

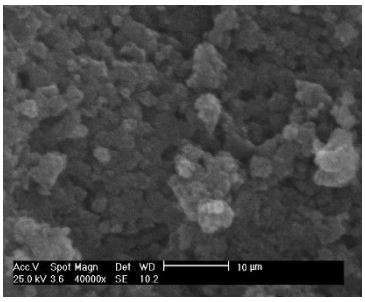

(d)

Fig. 4: The SEM images of Titania particles. (a) primary NPs, (b) aggregates, (c) simple-agglomerates and (d)complex-agglomerates.

The critical gas velocity is important to obtain a minimum size of NP agglomerate. The relationship between the pressure drop and superficial gas velocity (characteristics curve) has been described by the Ergun's equation [37]:

$$\frac{\Delta P}{H_0} = 150\frac{(1-\varepsilon)^2}{\varepsilon^3}.\frac{\mu_g U_g}{d_{agg}^2} + 1.75\frac{1-\varepsilon}{\varepsilon^3}.\frac{\rho_g \mu_g U_g^2}{d_{agg}} \qquad (18)$$

Where H_0 is the initial bed height, ε is the porosity (voidage) of the bed, μ_g is the viscosity of fluidizing gas and ρ_g is the gas density.

RESULTS AND DISCUSSION

Size Study of NPs, Aggregates and Agglomerates

Fig. 4 shows the SEM images of (a) Titania NPs, (b) aggregates, (c) simple-agglomerates and (d) complex-agglomerates. It expected that the complex-agglomerates essentially were found in the bed bottom because of their high density. Fig. 4a shows the primary Titania NPs are found in rigid crystals with primary sizes varies from ~15 to 90 nm due to the presence of strong interparticle forces. Fig. 4b shows the porous structure of aggregates consists of hierarchical clusters, which have tens of micrometers in size. The primary NPs stick to each other to form aggregates with low apparent density and rough surfaces (Fig. 4b). Fig. 4c shows the simple-agglomerates with different sizes of ~10 to 50 µm that formed from aggregates. The surfaces of the simple-agglomerates are much rougher than those of aggregates, and the interaction between the simple-agglomerates could be completely different from that between aggregates [31, 38]. Much void space was seen between the joined simple-agglomerates, which was due to the lower bulk density of these structures is compared with the aggregates. Fig. 4d shows the complex-agglomerates in the size ranges of ~100 to 300 µm, consisting of the simple-agglomerates. Based on the literature, the complex-agglomerates could be fluidized in the bed with the ABF regime [20, 21, 31]. Although the shape of simple-agglomerates and complex-agglomerates was not spherical exactly (Figs. 4c and 4d), a spherical shape was nearly considered for the real agglomerates. By supposing that the fluidized agglomerates have a spherical shape, the equivalent diameter was respected as an average diameter of agglomerates [14].

Dynamical study of agglomerates size

Fig. 5 shows the time variation of the Titania agglomerate diameter in the bed fluidized by nitrogen gas

and airflow at U_g of 1.0 m/s and H_0=0.04 m, where the laser probe was placed at height of 25 cm above the gas distributor. Error bars represent the standard deviation arising from at least four experimental data. It can be seen that the diameter of the agglomerates fluctuate non-linearly with fluidization time. At first, the diameter of the agglomerates increases abruptly and then reaches a dynamic equilibrium state associated with size fluctuations in the diameter range of ~170-230 µm. The agglomerates were continuously broken apart and form again to keep a dynamic equilibrium state between inertial and cohesive forces in the bed. Before reaching the dynamic equilibrium state, the agglomerates' diameter varied in the range of less than one hundred micrometers or more, which indicates the complex agglomerates (d_{agg}>100 µm) were in dynamical equilibrium with the simple-agglomerates (d_{agg} <100 µm) continuously because of the recombination and the breakage during the fluidization of NPs. After reaching the dynamic equilibrium state, the bed fluidized by the airflow has higher fluctuations in size than the bed fluidized by the nitrogen gas, indicating the widespread PSD and formation of large agglomerates (Fig. 5). As the large agglomerates circulate in the bed, break into smaller ones and again the smaller ones recombine continuously to form new larger agglomerates. The time-averaged mean diameter of agglomerates fluidized by nitrogen gas and air flow was 180±10 and 205±18 µm, respectively.

Fig. 6 illustrates the size distribution of agglomerates resulted from bed fluidized by airflow (a) and nitrogen gas (b) at U_g=1.0 m/s. The size of agglomerates varies from 30 to 450 µm. The results generated by the laser technique and analyzed by image processing software at different places of the fluidized bed. The results showed a rise in the quantity of the simple-agglomerates (<100 µm) associated with a remarkable decrease in the complex-agglomerates (>100 µm) when nitrogen was used. The distribution of agglomerates was dissimilar along with the axial direction of the bed, where the large and heavy agglomerates tended to descend to the bottom and fine particles remained at the bed surface. The size distribution curves exhibit an axis-symmetric trend for both atmospheres (Fig. 6). However, more homogeneity in size distribution of the agglomerates was seen in the bed fluidized by airflow. Image analysis of the bed fluidized by airflow illustrated that the diameters of the simple-agglomerates and complex-agglomerates were in the ranges of 60±15 µm and 270±30 µm, respectively. Similarly, when nitrogen

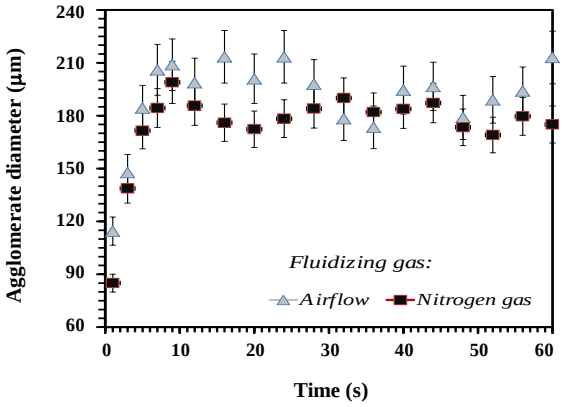

Fig. 5: The time variation of the Titania agglomerate diameter in the bed fluidized by nitrogen gas and airflow at U_g of 1.0 m/s and H_0=0.04 m [Error bars represent the standard deviation arising from at least four experimental data].

was used, the mean sizes of simple-agglomerates and complex-agglomerates were 45±10 µm and 230±15 µm, respectively. The high inconsistency in the results could be attributed to the sintering of particles.

Morphological Study of Agglomerates

Fig. 7 shows the histogram of the sphericity of Titania agglomerates fluidized by airflow (a) and nitrogen gas (b) at U_g=1.0 m/s. Most of the agglomerates had sphericity between 0.60 and 0.95 when both airflow and nitrogen were used as fluidizing gas. The average sphericity of agglomerates fluidized by airflow and nitrogen gas was 0.79 and 0.83, respectively. This revealed that the shape of agglomerates was almost spherical. This minor difference between the agglomerate sphericities was because of adsorbed oxygen or the existence of humidity in the gas affecting the cohesive inter-particle forces [18, 19]. The estimated fractal dimension and prefactor of Titania agglomerates with the sphericity of 0.79 are 2.25±0.02 and 16±2, while the corresponding values for sphericity of 0.95, they were 2.23±0.02 and 18±3, respectively. This result showed that the influence of the sphericity value on the estimation of the fractal dimension of the complex-agglomerates was minor as compared to the uncertainties of the mentioned parameter. Therefore, mean sphericity of 0.81 was selected for the fractal scaling analysis.

Fractal Scaling Analysis of Agglomerates

Fig. 8 illustrated the variation of the number of the particles as a function of gyration diameter of Titania NP

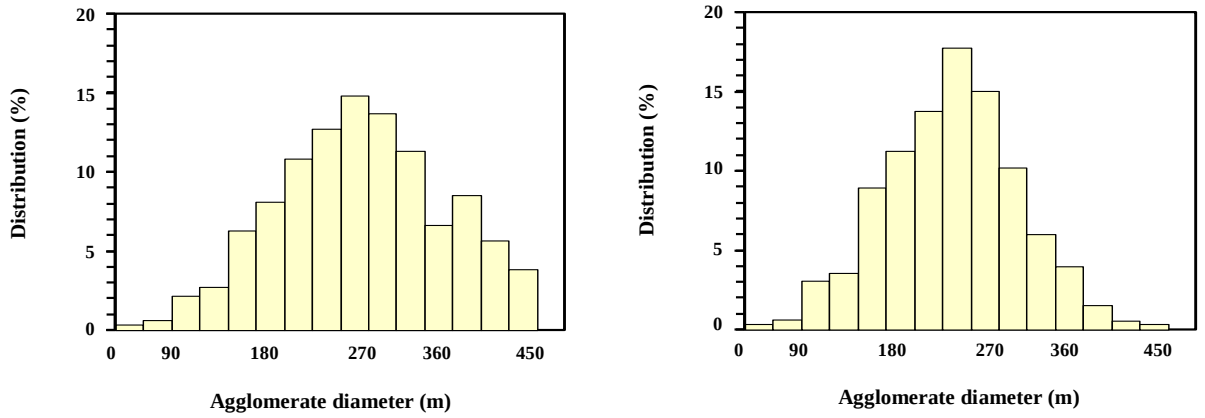

Fig. 6: The size distribution of Titania NP agglomerates obtained from bed fluidized by airflow (a) and nitrogen gas (b) at U_g=1.0 m/s.

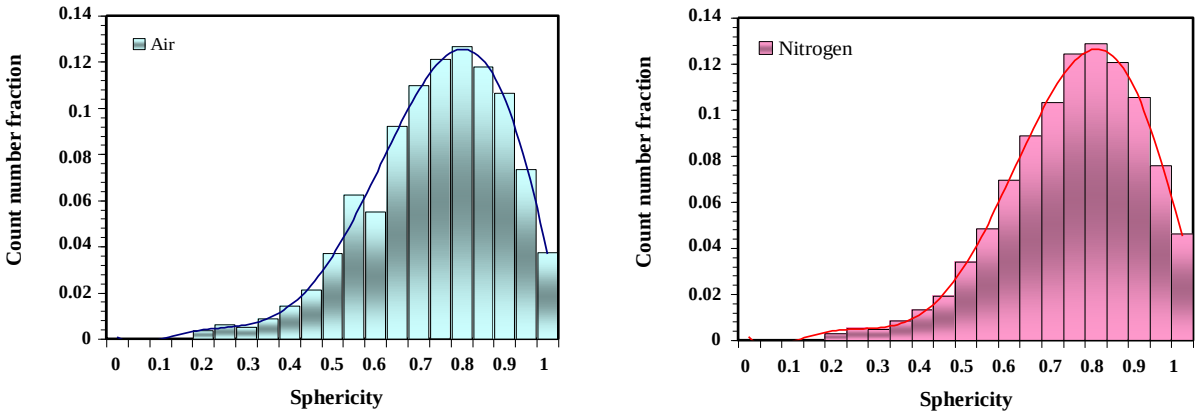

Fig. 7: The histogram of the sphericity of Titania NP agglomerates fluidized by air flow (a) and nitrogen (b) at ambient condition and U_g=1.0 m/s.

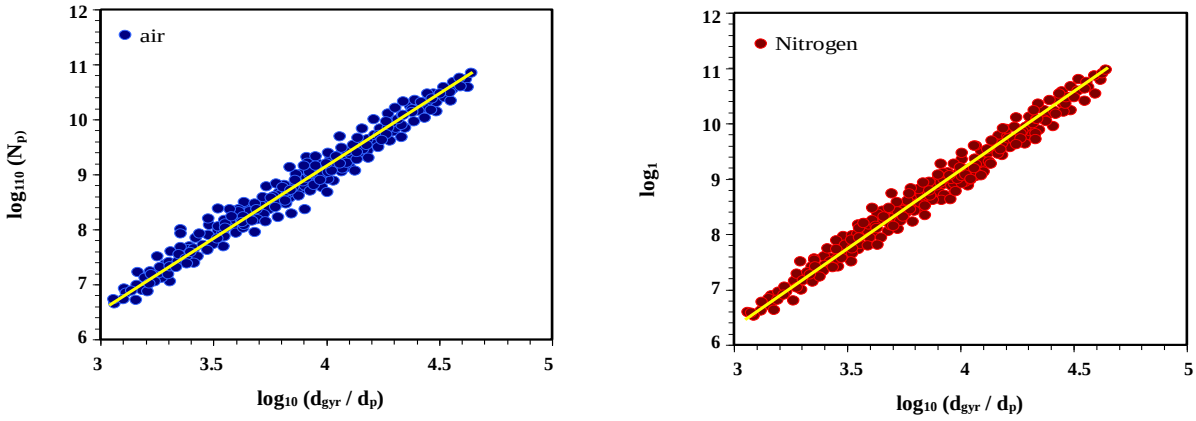

Fig. 8: The variation of the number of particles as a function of gyration diameter of Titania NP agglomerates fluidized by airflow (a) and nitrogen gas (b) at U_g=1.0 m/s [Yellow lines represent the best-fit line obtained by least square method].

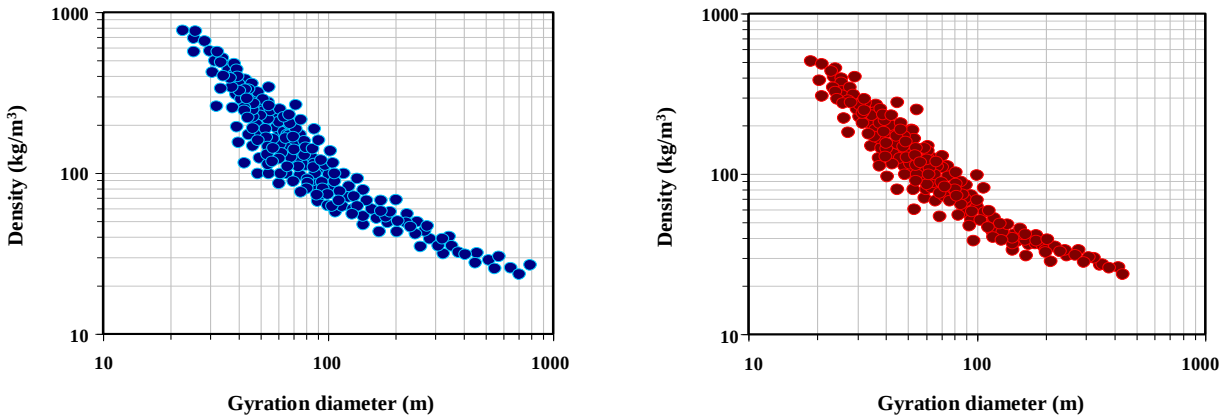

Fig. 9: The variation of the density of particles as a function of gyration diameter of Titania NP agglomerates fluidized by airflow (a) and nitrogen (b) at U_g=1.0 m/s.

agglomerates fluidized by airflow (a) and nitrogen gas (b) at U_g=1.0 m/s. The plots of $\log_{10}$ (N_p) vs. $\log_{10}$ (d_{gyr}/d_p) shows a linear relationship. The difference in results of gyration diameters of agglomerates fluidized by air and nitrogen was approximately less than 23% and 12%, respectively. Therefore, it would look nearly to have a similar value if equivalent diameters were used, instead of gyration diameter. The prefactor "k_n" and the fractal dimension calculated from the fitting curve were determined to be 11±3 and 2.15±0.07 for agglomerates fluidized by air, while the corresponding values were 9±2 and 2.21±0.05 for agglomerates fluidized by nitrogen, respectively. The obtained fractal dimensions were less than the value of 2.5-2.6 commonly reported in the literature [19, 20, 25]. The range of ~2.15<D_f<2.21 corresponds to the cluster-cluster reaction-limited mechanism of simple-agglomerates to the formation of complex-agglomerates [24]. This finding was consistent with the SEM analysis.

Fig. 9 shows the variation in the density of particles as a function of the gyration diameter of Titania NP agglomerates fluidized by airflow (a) and nitrogen gas (b) at U_g=1.0 m/s. The logarithm of the density of the particles confirms a linear relationship with the logarithm of the agglomerate gyration diameter in the sizes range of 20-230 µm. There was a minor difference between the density of Titania NP agglomerates fluidized by airflow and nitrogen in the studied size range, although their bulk density is 210 and 185 kg/m^3, respectively [31]. The high density of complex-agglomerates fluidized by airflow led to the high value of the prefactor index, which might be the result of a compact structure of Titania agglomerates fluidized by airflow. The density of simple-agglomerates and complex-agglomerates can be approximated by using k_n=1 in Equation (1). Nevertheless, the densities estimated by these two fractal dimensions were completely different. The difference in bulk density was larger than that of the calculated for dense particles, which indicated that it should be careful to use the density of the agglomerates as the bulk density in the calculation of the fractal dimension [17, 18].

Table 1 shows the prefactor and fractal dimension exponents calculated by the logarithm of Eq.(1) to the experimental data. The error on the prefactor was considerable because it was determined by the line intercept on the log (ρ_a/ρ_p) axis and the error propagation from the uncertainty in the determination of the agglomerate density. The fractal dimension exponent of 2.4-2.5, comes from using k_n=1 in Eq. (1), the number of particles obtained by image analysis and the approximate density of agglomerates in the studied size range. The low sensitivity of the fractal dimension exponent related to large variations in the density of agglomerate was an agreement with the D_f=2.5 for fluidized NP agglomerates [11, 19]. A D_f=2.5 was accepted to illustrate the complex-agglomerates, corresponding to the diffusion-limited model of the particle-cluster formation mechanism. This result exhibited that the fractal dimension directly obtained by individual NPs. *Nam et al.* [1] used the bed settling experiments to the determination of the size and the fractal dimension

Table 1: The prefactor and fractal dimension exponents of NP agglomerates calculated by Eq. 1 to the experimental data.

Fluidizing gas	k_n (-)	D_f (-)	Data points
Air	15±3	2.4±0.1	6578
Nitrogen	47±5	2.5±0.2	2045

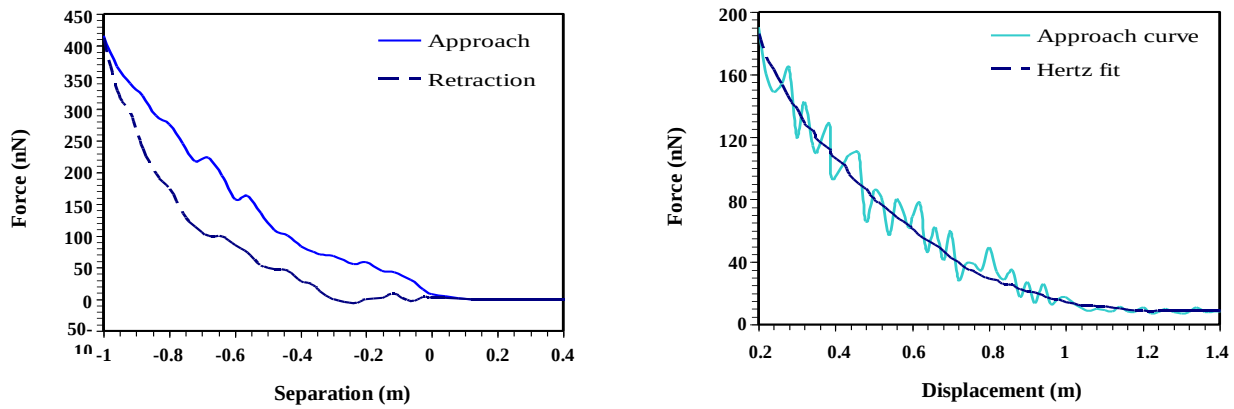

Fig. 10: Size estimation of agglomerates, (a) the force curves analysis of Titania agglomerates measured by AFM-based nanoindentation test. (b) Force-displacement curve [The force curve based on Hertz fit model].

of Aerosil R974 NP agglomerates. Their results showed the mean size and fractal dimension of agglomerates were 160 µm and 2.57, respectively. *Wang et al.* [11] reported a mean D_f=2.5 for Aerosil R974 NP agglomerates with similar agglomerate sizes; where the difference was less than 3 % with D_f=2.57.

Force Curve Analysis of NPs and Agglomerates

Fig. 10 shows the force curve analysis (a) and force-displacement curve (b) of Titania agglomerates measured by the AFM-based nanoindentation test. There was a large hysteresis between the slope of approach and retraction sections, which represents the porous structure of agglomerates. Based on the curve (Fig. 10a), approximately 1 µm of indentation depth is required to obtain the 450 nN compression force. The mentioned indentation depth corresponds to a chain structure consisting of 30 NPs with 0.5% of the complex-agglomerate size. To study the elasticity of porous particles, the approach section was analyzed [29]. Because of the complexity of the retraction curve, which consists of short-range adhesion forces among the agglomerates, a deformation of the agglomerates will be expected in the retract section. The approach section of the force curves was fitted by the Hertz model to calculate elastic Young's modulus of agglomerates [35, 39]. The Hertz fit was obtained based on the approach curve of a force-displacement curve. A specific quantity of approach section (<33%) associated with an inaccurate fit of the Hertz model was sufficient to represent the plastic deformation of agglomerates (Fig. 10b). The results showed that a wide range of Young's modulus in the limit of 20-200 kPa (Fig. 10), which was in the same order of magnitude as those predicted by the "Kendall" model used for the porous structures [40]. The wide distribution of Young's modulus may be explained as follows. The first reason was due to the different number of NPs approaching into the contact zone at each measurement. The second reason was explained based on the nature of porous agglomerates, wherein the contact zone there was a deviation from experiments because of the surface of the agglomerate was rather heterogeneous structure. The interparticle force of Titania NP agglomerates was significant because of the hydrophilic nature, where the interparticle forces decrease with increasing the size of agglomerates. The low Young's modulus of large Titania agglomerates showed that the material was easier to compress.

Size estimating of agglomerates

Fig. 11 shows the prediction curve of the size agglomerate for Titania agglomerate fluidized at various

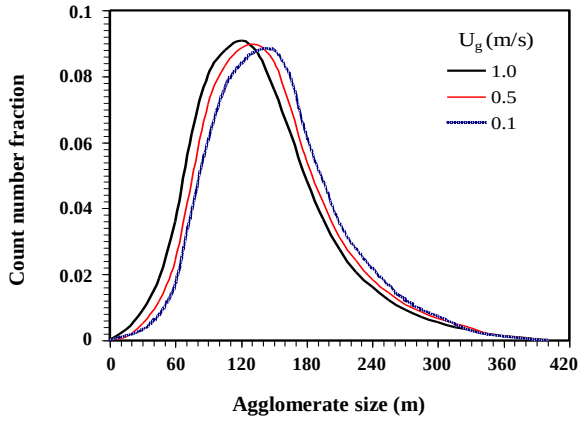

Fig. 11: The prediction curve of the size agglomerate for Titania fluidized at different U_g.

U_g of 0.1, 0.5 and 1.0 m/s. The agglomerate size distribution predicted by the model covered a wide range corresponding to a Gaussian function. It was expected that the estimated agglomerate sizes were smaller than those reported by experiments. This led to an error in the estimation of agglomerate size obtained by our force balance model at different gas velocities. It could be found that the predicted agglomerate size slightly decreased from 153 to 122 µm, when the gas velocity increased from 0.1 to 10 m/s, respectively. This trend was because of the change in the acting forces on the agglomerates at various hydrodynamic conditions. By increasing the U_g, the drag force exercised on the agglomerates increases slightly, while the van der Waals force was independent of the U_g. Thus, the size of agglomerates reduced when an increase of the separation forces.

Table 2 shows the mean standard deviation μ and the relative standard deviation σ of the proposed model at different gas velocities under ABF fluidization. The ratio of the d_{agg} at the mode ($d_{agg\ (Mode)}$) to the variation point ($d_{agg\ (Max)}$), which indicated by δ, was also shown in this table. As can be seen, the mean and relative standard deviation is increased when gas velocity increased. These results showed that a non-uniform ABF fluidization behavior was recognized by increasing the gas velocity, which was expressed by channeling and plugs associated with an eruption of large bubbles at the splash zone [41]. Based on the mode to infection point ratio δ analysis, there was a relative agreement with the size distribution based on the experimental data and the presented model. The following aspects were interesting to respect. At first, the predicted model at U_g=0.1 m/s leads to the size distribution of a δ= 0.54, whereas at U_g=0.5 m/s with more uniform fluidization gives a ratio of 0.64. The second aspect was the absolute values of agglomerate sizes. The error comes from the selection of agglomerate sampling technique after fluidization experiments by measuring from the splash zone. The distribution of agglomerates was not uniform along with the bed height, where the splash zone almost contains simple-agglomerates that simply fluidized on the bed surface by the inertial force generated by gas flow, while the model predicted the agglomerate size without any adjustable parameters and that it uses independently determined particle properties. The third source of error comes from the sample preparing method for the SEM analysis. Since in imaging analysis, particles were collected together, it could be expected that the size of complex-agglomerates measured by SEM analysis was larger than the mean values of the obtained in the bed by laser imaging.

Fig. 12 shows the parity plot of experimental data onto Titania agglomerates fluidized by air and nitrogen and calculated the average size of agglomerates obtained by the proposed model (dark, grey and white colors represent U_g of 0.1, 0.5, and 1.0 m/s, respectively). It could be found that the distribution of the results in the parity plot was unbiased and they were distributed over a negative deviation ~12% for nitrogen and ~30% for airflow, which indicated the underestimation of predicted agglomerate size. However, the agglomerate size distribution predicted by the model at U_g=1.0 m/s showed a higher deviation than that of the result obtained at U_g=0.1 m/s. The discrepancy between the experimental data and the predicted model could be ascribed to assumptions of the force balance model. The mean values of related parameters such as the equivalent diameter were used to estimate the mean agglomerates diameter, while the experimental data will give the exact value. The results showed that the proposed model could better estimate the agglomerates size of Titania NPs fluidized by nitrogen gas than the airflow. The results also confirmed that the large agglomerate sizes were obtained at high gas velocities.

Fig. 13 shows the characteristics curve (ΔP-U_g) of the bed fluidized at H_0=0.04 m. It can be seen that as gas velocity increases, the pressure drop increases to reach a maximum value corresponding to U_{mf}=0.4 m/s, then the pressure drop decreases to reach an approximately

Table 2: The mean standard deviation μ, the relative standard deviation σ, and the ratio of the d_{agg} at the mode to variation point of model at different gas velocities under ABF fluidization.

U_g (m/s)	μ	σ	δ
0.1	4.96	0.42	0.54
0.5	5.32	0.44	0.64
1.0	5.87	0.50	0.59

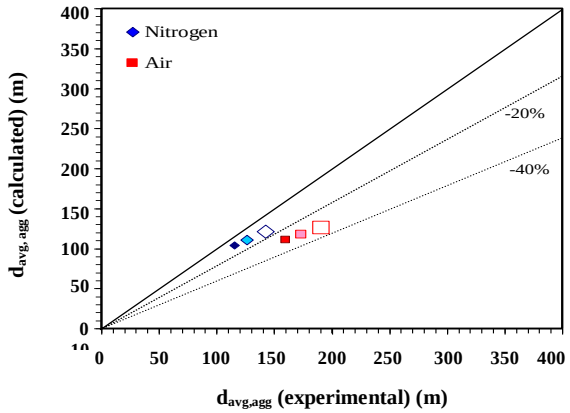

Fig. 12: The parity plot between experimental data and calculated average size of Titania NP agglomerates fluidized by nitrogen and air (dark, grey and white colors represent U_g of 0.1, 0.5, and 1.0 m/s, respectively).

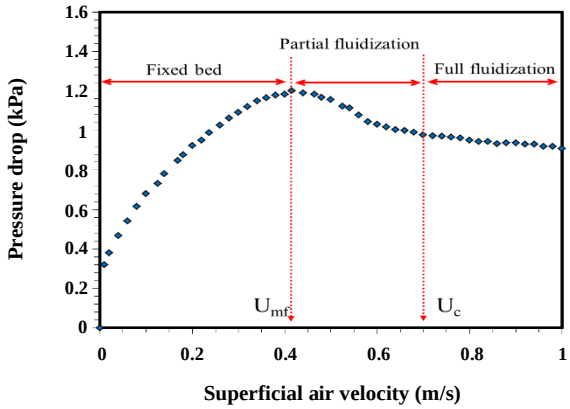

Fig. 13: The characteristics curve (ΔP-U_g) of the bed fluidized at H_0=0.04 m.

constant value. At $U_g \geq 0.7$ m/s, the flow regime changes from partial fluidization to a full fluidization state. According to Ergun's equation, pressure drop over bed height was not affected by an inertial force effect when the superficial velocity was larger than U_{mf}. At $U_g \geq 0.7$ m/s, the pressure drop of the bed was almost independent of the superficial gas velocity, while the average size of the complex-agglomerates gradually increases. Therefore, it can be concluded that the U_g=0.5 m/s is defined as the critical gas velocity.

CONCLUSIONS

The size estimating of fluidized Titania nanoparticle (NP) agglomerates were studied by force balance model and the fractal scaling analysis. The bed characteristics of fluidized Titania NPs with a mean primary size of 21 nm were studied in a conical bed by nitrogen and airflow at different gas velocities. The characteristic curve (ΔP-U_g) of the bed fluidized at an initial static bed height of 0.04 m was studied to find the minimum fluidization velocity and full fluidization state. The SEM images showed Titania NPs tended to link together with multi-stage agglomerates mechanism by three steps, including formation of aggregates with sizes of several hundred nanometers, simple-agglomerates with the sizes of ~5–20 μm, and complex-agglomerates with the sizes of ~100-300 μm. The results confirmed that the porous structure of simple-agglomerates lead to the lower bulk density of these structures was compared with the aggregates, while complex-agglomerates were light and fragile structure and have limited connecting sites between each other. The laser dynamic imaging results showed that the complex-agglomerates frequently broke at high gas velocities, reforming dynamically as new agglomerates with more porous structures. Owing to channeling into or near the bed walls, the complex-agglomerates were in dynamical balance with the porous simple-agglomerates. The probability size distributions of agglomerate changed with gas velocity, where more bed homogeneity was seen at high gas velocities. The sphericity analysis showed that most of the agglomerates had sphericity between 0.60-0.95 (mean sphericity of 0.83), suggested that the complex-agglomerates were nearly spherical. The fractal dimension

analysis was used through a linear relationship between the numbers of particles with the gyration diameter of complex-agglomerates. The values of the prefactor and fractal dimension of complex-agglomerates calculated by the fitting curve determined to be 11±3 and 2.15±0.07 for agglomerates fluidized by airflow, while the corresponding values were 9±2 and 2.21±0.05 for agglomerates fluidized by nitrogen gas, respectively. The D_f~2.2 represents the cluster-cluster reaction-limited mechanism to the formation of complex agglomerates. The force-displacement curve obtained by the nanoindentation test showed a wide distribution of Young's modulus in the range of 20-200 kPa, which corresponds to the porous structure of agglomerates.

In the theoretical section, a mathematical model based on the separation and adhesion forces balance was proposed to estimate the equilibrium size and size distribution of agglomerates in the bed. The effect of the collision force between the agglomerates and the van der Waals force was considered in the proposed model. The model predicted the size of agglomerates in the flow regime of the agglomerate bubbling fluidization. The prediction of the agglomerate size distribution was close to the experimental data obtained for fluidization by nitrogen gas. The results of this study can help to determine the critical gas velocity in achieving the desired agglomerate size of Titania NPs.

Acknowledgment

The author should like to thanks the Hamedan University of Technology (HUT, Grant No. 980701) and the Iran National Science Foundation (INSF) organization for their support (Grant No. 97012847).

Received : Sept. 6, 2019 ; Accepted : Jan. 13, 2020

REFERENCES

[1] Nam C.H., Pfeffer R., Dave R.N., Sundaresan S., Aerated Vibrofluidization of Silica Nanoparticles, *AIChE J*. **50(8)**: 1776-1785 (2004).

[2] Yao W., Guangsheng G., Fei W., Jun W., Fluidization and agglomerate structure of SiO_2 nanoparticles, *Powder Technol*. **124(1-2)**: 152-159 (2002).

[3] Hotze E.M., Phenrat T., Lowry G.V., Nanoparticle Aggregation: Challenges to understanding transport and reactivity in the environment, *J. Environ. Qual*. **39(6)**: 1909-1924 (2010).

[4] Bashiri H., Mostoufi N., Sotudeh-Gharebagh R., Chaouki J., Effect of Bed Diameter on the Hydrodynamics of Gas-Solid Fluidized Beds, *Iran. J. Chem. Chem. Eng. (IJCCE)*, **29(3)**: 27-36 (2010).

[5] Fotovat F., Ansart R., Hemati M., Simonin O., Chaouki J., Sand-Assisted Fluidization of Large Cylindrical and Spherical Biomass Particles: Experiments and Simulation, *Chem. Eng. Sci*. **126(1)**: 543-559 (2015).

[6] Sun G., Grace R., Effect of Particle Size Distribution in Different Fluidization Regimes, *AIChE J*. **38(5)**: 716-722 (1992).

[7] Geldart D., Types of Gas Fluidization. *Powder Technol*. **7(5)**: 285-292 (1973).

[8] Jing S., Hu, Q., Wang J., Jin Y., Fluidization of Coarse Particles in Gas-Solid Conical Beds, *Chem. Eng. Process*. **39(4)**: 379-387 (2000).

[9] Castellanos A., Valverde J.M., Quintanilla M.A.S. Physics of Compaction of Fine Cohesive Particles, *Phys. Rev. Lett*. **94(7)**: 075501 (2005).

[10] de Martin L., Sanchez-Prieto J., Hernandez-Jimenez F., van Ommen J., A Settling Tube to Determine the Terminal Velocity and Size Distribution of Fuidized Nanoparticle Agglomerates, *J. Nanopart. Res*. **16(1)**: 1-9 (2013).

[11] Wang XS, Palero VSoria J, Rhodes MJ., Laser-Based Planar Imaging of Nano-Particle Fluidization: Part i: Determination of Aggregate Size and Shape, *Chem. Eng. Sci*. **61(16)**: 5476-5486 (2006).

[12] To D., Dave R., Yin X., Sundaresan S., Deagglomeration of Nanoparticle Aggregates Via Rapid Expansion of Supercritical or High-Pressure Suspensions, *AIChE J*. **55(11)**: 2807-2826 (2009).

[13] Van Ommen R., Valverde, J.M., Pfeffer R., Fluidization of Nanopowders: A Review, *J. Nanopart. Res*., **14(3)** :737-766 (2012).

[14] Hakim L.F., Portman J.L., Casper M.D., Aggregation Behavior of Nanoparticles in Fluidized Beds, *Powder Technol*. **160(3)**: 149-160 (2005).

[15] Laube J, Salameh S, Kappl M, Madler L, Ciacchi LC., Contact Forces between TiO_2 Nanoparticles Governed by Interplay of Adsorbed Water Layers and Roughness, *Langmuir* **31(41)**: 11288-11296 (2015).

[16] Pimpang P., Zoolfakar A.S., Wongratanaphisan D., Gardchareon A., Nguyen E.P., Zhuiykov S., Choopun S., Kalantar-Zadeh K., Atomic Force Microscopy Adhesion Mapping: Revealing Assembly Process in Inorganic Systems, *J. Phys. Chem. C*, **117(39)**: 19984-19990 (2013).

[17] Jiang Q., Logan B.E., Fractal Dimensions of Aggregates Determined From Steady-State Size Distributions, *Environ Sci. Technol*. **25(12)**: 2031-2038 (1991).

[18] de Martin L., Fabre A., van Ommen J.R., The Fractal Scaling of fluidized Nanoparticle Agglomerates, *Chem. Eng. Sci*. **112**: 79-86 (2014).

[19] Fabre A, Salameh S, Colombi Ciacchi L, Kreutzer M.T., van Ommen J.R. Contact Mechanics of Highly Porous Oxide Nanoparticle Agglomerates, *J. Nanopart. Res*. **18(1)**: 1-13 (2016).

[20] Fabre A., Steur T., Bouwman W.G., Kreutzer M.T., van Ommen J.R., Characterization of the Stratified Morphology of Nanoparticle Agglomerates, *J. Phys. Chem. C* **120(36)**: 20446-20453 (2016).

[21] Valverde J.M., Castellanos A., Fluidization of nanoparticles: A Modified Richardson-Zaki Law, *AIChE J*., **52(2)**: 838-842 (2006).

[22] Ehrl L., Soos M., Lattuada M., Generation and Geometrical Analysis of Dense Clusters with Variable Fractal Dimension, *J. Phys. Chem. B*, **113(31)**: 10587-10599 (2009).

[23] Quintanilla M.A.S., Valverde J.M., Castellanos A., Lepek D., Pfeffer R., Dave R.N., Nanofluidization as Affected by Vibration and Electrostatic Fields, *Chem. Eng. Sci*. **63(22)**: 5559-5569 (2008).

[24] Sorensen C.M., Roberts G.C., The Prefactor of Fractal Aggregates, *J Colloid Interf. Sci*. **186(1)**: 447-456 (1997).

[25] Jiang Q., Logan B.E., Fractal Dimensions of Aggregates Determined from Steady-State Size Distributions, *Environ. Sci. Technol*. **25(12)**:2031-2038 (1991).

[26] Nakamura H., Watano S., Fundamental Particle fluidization Behavior and Handling of Nano-Particles in a Rotating Fluidized Bed, *Powder Technol*., **183(3)**: 324-332 (2008).

[27] Zhou T., Li H.Z., Force Balance Modelling for Agglomerating Fluidization of Cohesive Particles, *Powder Technol*., **111(1-2)**: 60-65 (2000).

[28] van Ommen J.R., Mudde R.F., Measuring the Gas-Solids Distribution in Fluidized Beds-A Review. *Int. J. Chem. React. Eng*. (*IJCRE*), **6(1)**: 1-29 (2008).

[29] Rong W., Pelling A.E., Ryan A., Gimzewski J.K., Friedlander S.K., Complementary TEM and AFM Force Spectroscopy to Characterize the Nanomechanical Properties of Nanoparticle Chain Aggregates, *Nano Lett*. **4(11)**: 2287-2292 (2004).

[30] Bahramian A., Kalbasi M., CFD Modeling of TiO_2 Nano-Agglomerates Hydrodynamics in a Conical Fluidized Bed Unit with Experimental Validation, *Iran. J. Chem. Chem. Eng., (IJCCE)*, **29(2)**: 105-120 (2010).

[31] Bahramian A., Grace J.R., Fluidization of Ttitania Nanoparticle Agglomerates in a Bench-Scale Conical Vessel, *Powder Technol*. **310(1)**: 46-59 (2017).

[32] Brasil A.M., Farias T.L., Carvalho M.G., A Recipe for Image Characterization of Fractal-Like Aggregates, *J. Aerosol Sci*. **30(10)**: 1379-1389 (1999).

[33] Tamadondar M.R., Zarghami R. Boutou K., Tahmasebpoor M., Mostoufi N. Size Of Nanoparticle Agglomerates in Fluidization, *Can. J. Chem. Eng*. **94(3)**: 476-484 (2016).

[34] Zhang W., Noda R., Horio M., Evaluation of lubrication Force on Colliding Particles for DEM Simulation of Fluidized Beds, *Powder Technol.*, **158(1-3)**: 92-101 (2005).

[35] Bushell G., Yan Y., Woodfield D., Raper J., Amal R., On Techniques for the Measurement of the Mass Fractal Dimension of Aggregates, *Adv. Colloid Interface Sci*. **95(1)**: 1-50 (2002).

[36] Bergstrom L., Hamaker Constants of Inorganic Materials, *Adv. Colloid Interface Sci*. **70(1)**: 125-169 (1997).

[37] Ergun S., Fluid Flow Through Packed Columns, *Chem. Eng. Prog*. **48(2)**: 89-94 (1952).

[38] Masoodiyeh F., Karimi Sabet J. Mozdianfard M., Population Balance Modelling of Zirconia Nanoparticles in Supercritical Water Hydrothermal Synthesis, *Iran. J. Chem. Eng*. (*IAChE*), **38(4)**: 1-9 (2019).

[39] Ghorbani H., Sotudeh-Gharebagh R., Abbasi M., Zarghami R., Mostoufi N., Modeling of Vibration of a Fluidized Bed Cylindrical Shell, *Iran. J. Chem. Eng*. (*IAChE*), **10(2)**: 67-80 (2013).

[40] Kendall K., Alford N.M., Birchall J.D., Elasticity of Particle Assemblies as a Measure of the Surface Energy of Solids, *Proceedings of the Royal Society of London A*: *Mathematical. Phys. Eng. Sci*. **412(1843**): 269-283 (1987).

[41] Shabanian J., Jafari R., Chaouki J., Fluidization of Ultrafine Powders, *Int. Rev. Chem. Eng.* (*I.RE.CH.E.*), **4(1)**: 16-50 (2012).